Surface anchoring as a control parameter for shaping skyrmion or toron properties in thin layers of chiral nematic liquid crystals and noncentrosymmetric magnets

Andrey O. Leonov*

Chirality Research Center, Hiroshima University, Higashi-Hiroshima, Hiroshima 739-8526, Japan;
Department of Chemistry, Faculty of Science, Hiroshima University Kagamiyama, Higashi Hiroshima, Hiroshima 739-8526, Japan;
and IFW Dresden, Postfach 270016, D-01171 Dresden, Germany

(Received 8 June 2021; accepted 1 October 2021; published 13 October 2021)

Existence of topological localized states (skyrmions and torons) and the mechanism of their condensation into modulated states are the ruling principles of condensed matter systems, such as chiral nematic liquid crystals (CLCs) and chiral magnets (ChM). In bulk helimagnets, skyrmions are rendered into thermodynamically stable hexagonal skyrmion lattice due to the combined effect of a magnetic field and, e.g., small anisotropic contributions. In thin glass cells of CLCs, skyrmions are formed in response to the geometrical frustration and field coupling effects. By numerical modeling, I undertake a systematic study of skyrmion or toron properties in thin layers of CLCs and ChMs with competing surface-induced and bulk anisotropies. The conical phase with a variable polar angle serves as a suitable background, which shapes skyrmion internal structure, guides the nucleation processes, and substantializes the skyrmion-skyrmion interaction. I show that the hexagonal lattice of torons can be stabilized in a vast region of the constructed phase diagram for both easy-axis bulk and surface anisotropies. A topologically trivial droplet is shown to form as a domain boundary between two cone states with different rotational fashion, which underpins its stability. The findings provide a recipe for controllably creating skyrmions and torons, possessing the features on demand for potential applications.

DOI: 10.1103/PhysRevE.104.044701

I. INTRODUCTION

Multidimensional localized structures (e.g., two-dimensional skyrmions [1–3] and/or three-dimensional Hopfions [4,5]) are the focus of intense research in many fields of modern physics including condensed-matter physics, optics, biophysics, particle and nuclear physics, astrophysics, and cosmology [6–9]. Since the late 1960s, the *fundamental* interest in such localized solutions is related to the explanation of countable particles in continuous fields, the instabilities of which due the constraints of the Hobart-Derrick theorem [10] can be overcome, if the energy functionals contain, for example, contributions with higher-order spatial derivatives. These topological solitons, originally introduced by Skyrme in nuclear physics [11], found their way into condensed-matter physics [2,12,13], where they preserved their name, but acquired a different stabilization mechanism—energy terms linear with respect to spatial derivatives of order parameters [14,15]. A great deal of interest, in particular, is attracted by chiral skyrmions, which created a research boom in chiral liquid crystals (CLC) and noncentrosymmetric chiral magnets (ChM) and gained, not only fundamental physics importance, but generated enormous interest in their *applications* in information storage and processing devices [16,17] (in ChMs) as well as new modes of displays (in CLCs) [18].

In noncentrosymmetric magnetic materials, skyrmions are stabilized by specific Dzyaloshinskii-Moriya interaction (DMI) [14,15], which is phenomenologically expressed by the so called Lifshitz invariants (LI):

$$\mathcal{L}^{(k)}_{i,j} = M_i \frac{\partial M_j}{\partial x_k} - M_j \frac{\partial M_i}{\partial x_k}, \tag{1}$$

where M_i and M_j are components of magnetization vectors that arise in certain combinations depending on crystal symmetry and x_k are spatial coordinates. For cubic helimagnets belonging to 23 (T) (as MnSi, FeGe, and other B20 compounds) and 432 (O) crystallographic classes, Dzyaloshinskii-Moriya interactions are reduced to the following form:

$$W_{\mathrm{DM}} = D\left(\mathcal{L}^{(z)}_{yx} + \mathcal{L}^{(y)}_{xz} + \mathcal{L}^{(x)}_{zy}\right) = D\,\mathbf{M}\cdot \mathrm{rot}\mathbf{M}. \tag{2}$$

In chiral liquid crystals [19,20], the acentric shape of underlying molecules being at the heart of chiral effects leads to the same functional form of chiral interactions (2) for the molecular alignment field $\mathbf{n}(\mathbf{r})$.

To additionally control the structure and topology of localized particlelike states in CLCs and ChMs, one employs confinement effects with controllable boundary conditions and coupling to applied fields [21–23]. Magnetic skyrmions are commonly subjected to the effect of an applied magnetic field, which contributes a Zeeman energy to the energy functionals [24]. By the magnetic field, a hexagonal lattice of skyrmions may be rendered into a thermodynamically stable state. The existence region of isolated skyrmions (IS) becomes restricted by strip-out instabilities at low fields

*leonov@hiroshima-u.ac.jp

and a collapse at high fields [25]. The role of the surface-induced anisotropy (anchoring) on magnetic skyrmions is rather neglected by the magnetic skyrmionic community. Phenomenologically, such a surface anisotropy is known to appear due to the reduced coordination number at the surfaces of magnetic materials. Moreover, it can be modified by covering the magnetic layers with different nonmagnetic materials [26–28].

CLC skyrmions, on the contrary, are usually subjected to boundary conditions in the form of an easy-axis or easy-plane anisotropy (so called surface anchoring), since they are confined in a glass cell with thickness comparable with the helicoidal pitch [23,29–31]. Then, in principle, a Zeeman-like term absent in CLCs can be substituted by the interplay of an electric field, which fulfills the role of a bulk easy-plane or easy-axis anisotropy, and the surface anchoring acting in an opposite way [32,33]. This frustration would create a suitable environment for topologically nontrivial localized states within the conical or homogeneous state. Interestingly, in ferromagnetic CLCs formed by colloidal dispersion of magnetic monodomain nanoparticles, one may achieve a linear coupling and facile response to applied magnetic fields, as well [34,35]. These arguments facilitate the discussion of topological phases in CLCs and ChMs on the same footing. At the same time, the present manuscript allows one to highlight the historic obstacles CLC and ChM communities faced along the way by addressing the problem of soliton stability and topology.

In the present manuscript, I undertake a systematic study of skyrmion properties modified by the presence of defects and a conical state with a variable polar angle in chiral liquid crystals and chiral magnets. I notice that despite the well-documented importance of surface boundary conditions, their role in stabilizing different one-, two-, and three-dimensional solitonic CLC structures has not been systematically explored so far. Thus the first goal of this work is to study phase diagram and director or magnetization structures that appear because of geometrical frustration of CLCs and ChMs in thin cells with homeotropic and planar anchoring. In the next section, I introduce a phenomenological model and the algorithms used for numerical simulations. I plot the phase diagram of conical states in thin layers of CLCs and emphasize the structural differences with the cone states in ChMs. In Sec. IV by numerically solving the differential equations minimizing the phenomenological functional, I derive the equilibrium structures of confined isolated skyrmions as functions of the material parameters and applied electric fields. I discuss an anisotropic character of skyrmion interaction manifested by skyrmion chains. Since the defects formed within skyrmions by the strong surface anchoring have the ring shape and are energetically costly, the skyrmion lattice (SkL) is replaced by the lattice of torons that contain only two point defects near the surfaces (Sec. V). The complete phase diagram of states (Sec. VI) also exhibits one-dimensional (1D) straight and oblique spiral states. I discuss the first- and second-order phase transitions between these 1D modulations. I finalize the manuscript by considering the structure of 3D droplets with zero topological charge. Such droplets are shown to appear as a domain boundary between the conical states with different rotational structure. The topological charge is conventionally defined as a way of wrapping the sphere and it is calculated for different 2D crosscuts of obtained structures as

$$Q = \frac{1}{4\pi}\int \mathbf{m}\left(\frac{\partial \mathbf{m}}{\partial x} \times \frac{\partial \mathbf{m}}{\partial y}\right) dx\, dy, \tag{3}$$

where $\mathbf{m}$ stands for the director in CLC or the magnetization in chiral magnets. The topological charge is a quantity widely used in the skyrmionics community. Whenever possible, I also discuss connections of the theoretical results to the experimental findings in different condensed-matter systems.

II. PHENOMENOLOGICAL MODEL AND ONE-DIMENSIONAL SPIRAL STATES IN MAGNETS

The simplest model for *magnetic* states in bulk noncentrosymmetric ferromagnets is based on the following energy density functional [15,36]

$$w = A\,(\mathbf{grad}\,\mathbf{m})^2 + D\,\mathbf{m}\cdot \mathrm{rot}\,\mathbf{m}, \tag{4}$$

includes only the exchange stiffness with constant A and the Dzyaloshinskii-Moriya coupling energy with constant D, and

$$\mathbf{m} = (\sin\theta\,\cos\psi; \sin\theta\,\sin\psi; \cos\theta) \tag{5}$$

is the unity vector along the magnetization vector $\mathbf{M} = \mathbf{m}M$.

I also notice that the energy terms in model (4) correspond to the elastic energy contributions in the Frank-Oseen free energy [19] that pertain to splay K_1, twist K_2, and bend K_3 distortions of the director provided that the one-constant approximation $K_1 = K_2 = K_3 = K$ is utilized [20]: $A \to K/2$, $D \to Kq_0$ ($q_0 = 2\pi/p$ is the chiral wave number of the ground-state chiral nematic mixture; p is a helix pitch or the width of one complete turn of the director $\mathbf{n}$ along the helical axis). Indeed, the values of elastic constants in common CLCs are comparable and this one-constant approximation can be used to model their (ordinary) behavior. Commonly the Frank-Oseen free energy is used for orientable director fields $\mathbf{n}$. In this case, the director fields are dressed smoothly with vectors without introducing extra fictitious singularities [19]. In the following, I use the vector field $\mathbf{m}$ for both the magnetization and the director.

All solitonic structures discussed in this work are modeled by minimizing the free energy (4) with the constraint $|\mathbf{m}| = 1$, i.e., I avoid the "softening" of the magnetization modulus that has dramatic consequences near the ordering temperatures: in this case, skyrmionic textures consist of complex combinations of rotational and longitudinal modulations, the essence of aforementioned precursor effects [37,38]. At the same time, I notice that Landau–de Gennes modeling can be additionally used to properly model singular half-integer defect lines, in particular, in the cholesteric fingers of the third type (CF-3) [39]. The Landau–de Gennes modeling is based on a traceless and symmetric tensor Q_{ij} [19].

A. Helical modulations

In chiral magnets, the Dzyaloshinskii-Moriya interactions play a crucial role in destabilizing the homogeneous ferromagnetic arrangement and twisting it into a helix, which is a single-harmonic mode forming the global minimum of the functional (4) [15]:

$$\mathbf{M} = M[\mathbf{n}_1 \cos(\mathbf{q}\cdot\mathbf{r}) + \mathbf{n}_2 \sin(\mathbf{q}\cdot\mathbf{r})]. \tag{6}$$

$\mathbf{n}_1$, $\mathbf{n}_2$ are the unit vectors in the plane of the magnetization rotation orthogonal to the wave vector $\mathbf{q} = \mathbf{n}_3/L_D$ with $\mathbf{n}_3 \perp \mathbf{n}_2 \perp \mathbf{n}_1$ (i.e., $\mathbf{n}_1$, $\mathbf{n}_2$, and $\mathbf{n}_3$ are three mutually orthogonal unit vectors). L_D is proportional to the ratio of the counteracting exchange and Dzyaloshinskii constants and introduces a fundamental *length* characterizing the periodicity of chiral modulations in chiral magnets, $L_D = A/D$.

The helical modulations have a fixed rotation sense determined by the sign of Dzyaloshinskii-Moriya constant D and are continuously degenerate with respect to propagation directions of the helical modulations in space. An applied magnetic field lifts this degeneracy and stabilizes two types of one-dimensional modulations: cones and helicoids with propagation directions parallel and perpendicular to the applied magnetic field, respectively. An applied magnetic field $\mathbf{H}$ contributes the Zeeman energy term to (4) in ChMs,

$$w_Z = -\mu_0 M\mathbf{m}\cdot\mathbf{H}, \tag{7}$$

For helicoids, analytical solutions for the polar angle $\theta(x)$ of the magnetization written in spherical coordinates, $\mathbf{M} = M[\sin\theta(x)\cos\psi, \sin\theta(x)\sin\psi, \cos\theta(x)]$, are derived by solving a *pendulum* equation $A\, d^2\theta/dx^2 - H\cos\theta = 0$. Such solutions are expressed as a set of elliptical functions [15] and describe a gradual expansion of the helicoid period with increased magnetic field. In a sufficiently high magnetic field H_H the helicoid infinitely expands and transforms into a system of isolated noninteracting 2π-domain walls (kinks) separating domains with the magnetization along the applied field [2,15]. The dimensionless value of this critical field is

$$h_H = H_H/H_D = \pi^2/8 = 0.30843, \tag{8}$$

with $H_D = D^2/AM$. The azimuthal angle ψ, on the contrary, is fixed by the different forms of the Lifshitz invariants. In the considered case of cubic helimagnets $\psi = \pi/2$.

B. Conical state in chiral helimagnets

The wave vector of a conical state is oriented along the field. The conical state combines the properties of the ferromagnetic and the helical states as a compromise between the Zeeman and DMI energies and, as a solution with the period $p = 4\pi L_D$, exists below the critical field $H_C = H_D/2$. The equilibrium parameters for this cone phase are expressed in the analytical form [36] as

$$\theta_c = \arccos(2H/H_D), \quad \psi_c = 2\pi z/p_0, \tag{9}$$

with the constant polar angle θ_c and linearly varying azimuthal angle ψ_c. Above the critical field H_C the cone phase transforms into the saturated state with $\theta = 0$.

I also supplement the model (4) with the uniaxial anisotropy (UA) energy term

$$w_{ua} = -K_u(\mathbf{m}\cdot\mathbf{z})^2. \tag{10}$$

For the easy-plane UA, $K_u < 0$, the conical phase remains the global minimum in the whole region of the phase diagram [24,40]. An additional uniaxial anisotropy, $K_u > 0$, must be included to suppress the conical state and thus unveil the regions of SkL and helicoidal stability [24].

The problem of SkL stability in bulk chiral helimagnets originates from the phenomenon of the A phase. It was found that there are only small energy differences between various modulated states including skyrmions. On the other hand, weaker energy contributions, such as uniaxial (10) or cubic anisotropies, impose distortions on different modulated states and thus determine their stability limits on the corresponding phase diagrams. That is why in particular the uniaxial anisotropy of the easy-axis type, which does not affect the ideal single-harmonic type of the magnetization rotation in the conical spiral but just leads to the gradual closing of the cone, grants the thermodynamical stability to the SkL in a broad region of a theoretical phase diagram [24].

III. CONICAL STATE IN THIN LAYERS OF CHIRAL NEMATICS

In the following, I consider CLC sandwiched between two glass plates with the layer thickness T. When the surface anchoring energy is considered finite and taken into account, Eq. (4) is supplemented by the Rapini-Papoular surface anchoring potential:

$$W_s = -\int K_s(\mathbf{m}\cdot\mathbf{z})^2\, d^2\mathbf{r}, \tag{11}$$

where the easy axis orientation is chosen to be along $\mathbf{z}$, i.e., along the surface normal of the substrates. The type of anchoring (e.g., planar or homeotropic) is specified by the sign of the constant K_s.

All forthcoming calculations will be done for thin films with the ratio $T/4\pi L_D = 1$, although I discuss some implications for thicker samples. Solutions for particlelike skyrmions as well as for different modulated states are derived by minimization of Eq. (4) including the bulk w_{ua} (10) and surface w_s (11) uniaxial anisotropy terms with both signs of the constants K_u and K_s. In CLC, the uniaxial anisotropy is imposed by, e.g., an applied electric field $\mathbf{E}$ and has the same functional form as (9): $-(\varepsilon_0\Delta\varepsilon/2)(\mathbf{n}\cdot\mathbf{E})$, where $\Delta\varepsilon$ is the dielectric anisotropy. The Zeeman term w_z (7) is omitted henceforth. Besides, in usual apolar nematic liquid crystals, such a linear coupling does not exist, which additionally justifies its omission.

The complexity of many CLC structures also involving defects usually does not allow simple analytic descriptions of the director configuration. Therefore, I use numerical routines with finite-difference discretization on rectangular grids with adjustable grid spacings and periodic boundary conditions in the plane xy. The minimization procedure is described in detail in Refs. [41]. The solutions depend on the two control parameters, the reduced value of the bulk uniaxial anisotropy, K_uA/D^2, and the value of the reduced surface anchoring, K_sL_D/A, with the fixed thickness of the layer. In the following, the spatial coordinates are measured in units of L_D. In this paper, I also neglect effects imposed by spatial inhomogeneity of the induced anisotropy as well as the surface terms, e.g., K_{13} or K_4 [19]. The steep magnetization gradient close to the Bloch point can be addressed by atomistic modeling of the region close to the defect center [42]. However, a recent comparison

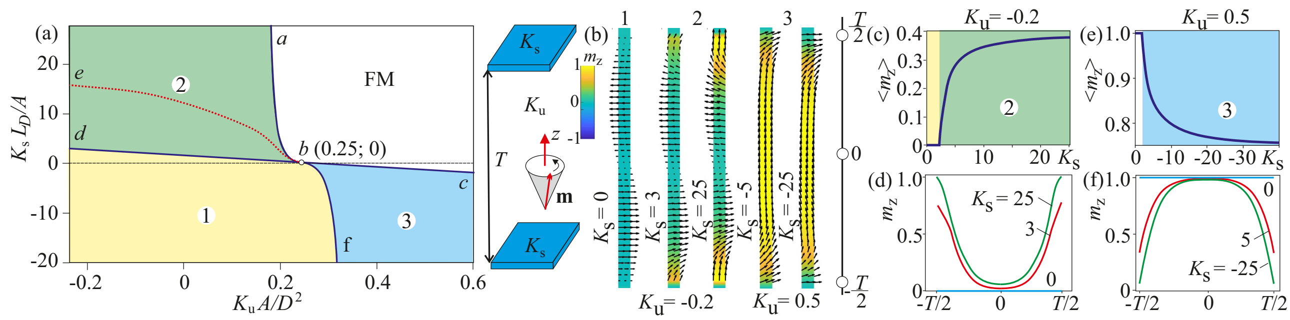

FIG. 1. Diagram of the cone solutions for model (4) in the space of control parameters $(K_u - K_s)$ and fixed value of the thickness, $T = 4\pi L_D$. Filled areas designate the regions, where the conical state has distinct internal structure: in region 1 (yellow shading), the conical state is flat across the layer thickness with $\theta_c = \pi/2$; in region 2 (green shading), the magnetization near the surfaces starts to align along z in response to the increasing homeotropic anchoring (line b–d). At the line b–e, the spins at the surface point along z and the conical structure is practically frozen. In region 3 (blue shading), the surface states acquire flat structure due to the planar anchoring, whereas the spins in the middle of the layer are in the homogeneous state along z. The color plots in (b) exhibit m_z component in all aforementioned conical states. Black arrows show projection of the magnetization onto the xz plane. Average magnetization $\langle m_z \rangle$ for the conical state is plotted within the regions 1–2 (c) and 3 (e) in dependence on the surface-induced anisotropy K_s for fixed values of the bulk anisotropy K_u. The surface anchoring leads to the saturation of $\langle m_z \rangle$ with the magnitude different from the FM state in (c) and/or planar cone in (e): once the surface states are formed according to the strong anchoring, the core structure within the layer does not change. Magnetization profiles plotted for several values of K_s in (d) and (f) show that the surface states almost do not intersect and the state in the middle of the layer is fully specified by the bulk anisotropy K_u.

between micromagnetics and atomistic simulations indicated that the two approximations come to a quantitative agreement when the micromagnetic simulation cell is comparable to the lattice constant [43,44].

As shown in Fig. 1, the cone angle θ_c in thin layers does not maintain its constant value (9) and effectively changes across the CLC cell thickness. But only at the line a–b–c can the cone transform into the homogeneous state as would be easily achieved by the magnetic field in Eq. (9). Within the present model system, however, both easy-axis bulk and surface anisotropies are needed for such a process. In the yellow-shaded region 1 with the easy-plane bulk anisotropy, the conical state retains the flat structure with $\theta_c = \pi/2$. And some finite value of easy-axis surface anisotropy K_s is required to force the magnetization out of the xy plane, which occurs at the line b–d. At the line b–e, the magnetization at the surface is fully aligned, $\theta_c(z = \pm T/2) = 0$, whereas within the layer interior the magnetization undergoes a rotation and is almost horizontal in the middle of the layer even for relatively large values of K_s, $\theta_c(z = 0) \approx \pi/2$ [see the magnetization profiles in Fig. 1(d)]. According to Fig. 1(c), the average m_z component for such conical profiles also saturates for increasing K_s value.

For the case of easy-axis bulk anisotropy (region 3), the easy-plane surface anisotropy cants the magnetization near the surfaces until it is fully horizontal with $\theta_c(z = \pm T/2) = \pi/2$ (line b–c). The magnetization profiles in Fig. 1(f) demonstrate the finite penetration depth of such surface states. According to Fig. 1(e), the average m_z components also saturate at some finite K_s values. With the decreasing value of K_u, however, the saturation occurs at smaller values of $\langle m_z \rangle$. And eventually, at the line b–f, the conical state again acquires a flat structure with the constant polar angle $\pi/2$. Analytical solutions for such conical states resemble the solutions for so called chiral surface twists formed at the free boundaries of cubic helimagnets and have the form of kink solitons of the double sine-Gordon model (see for details, e.g., Refs. [45–47]).

IV. ISOLATED SKYRMIONS WITHIN THE CONICAL STATE OF CLC

The conical phase in thin CLC layers represents an interesting medium to accommodate isolated skyrmions and to shape their intrinsic properties. The internal patterns of ISs with their axes along the wave vector of the conical phase in each region of the phase diagram [Fig. 1(a)] are depicted in Figs. 2 and 3 and exhibit a distinct variety of particlelike states.

A convenient way to depict these skyrmions, which has been proven to be particularly illustrative in addressing the character of skyrmion-skyrmion interaction, is as follows [41]. I extract the spins corresponding to the conical phase in accordance with the following criterium:

$$\left| m^i(\mathbf{r}) - m^i_c(\mathbf{r}) \right| < \epsilon, \qquad (12)$$

where $m^i(\mathbf{r})$ and $m^i_c(\mathbf{r})$ are the components of the magnetization within the skyrmion and the conical states, $i = x, y, z$; ϵ represents a required accuracy: the smaller ϵ is, the more spins are retained within the skyrmion structure. Then, I plot the remaining spins as spheres colored according to their m_z component [e.g., a 3D skyrmion model depicted in Fig. 2(a)].

In this way, all intricate details of the internal structure are explicitly revealed: skyrmions are composed of a cylinderlike (blue) core centered around the magnetization opposite to z and a (red) coil with the magnetization along the z axis. At the same time, I also plot skyrmion crosscuts along the different directions including all the spins [e.g., Fig. 2(b)]. Many ongoing experimental attempts are particularly focused on unveiling the three-dimensional spin texture of such skyrmion tubes [48–51].

A. Anisotropic character of skyrmion interaction manifested by skyrmion chains

The skyrmion-skyrmion interaction within the conical phase in regions 1 and 2 is argued to have an anisotropic character: it is attractive but with the largest energy reduction

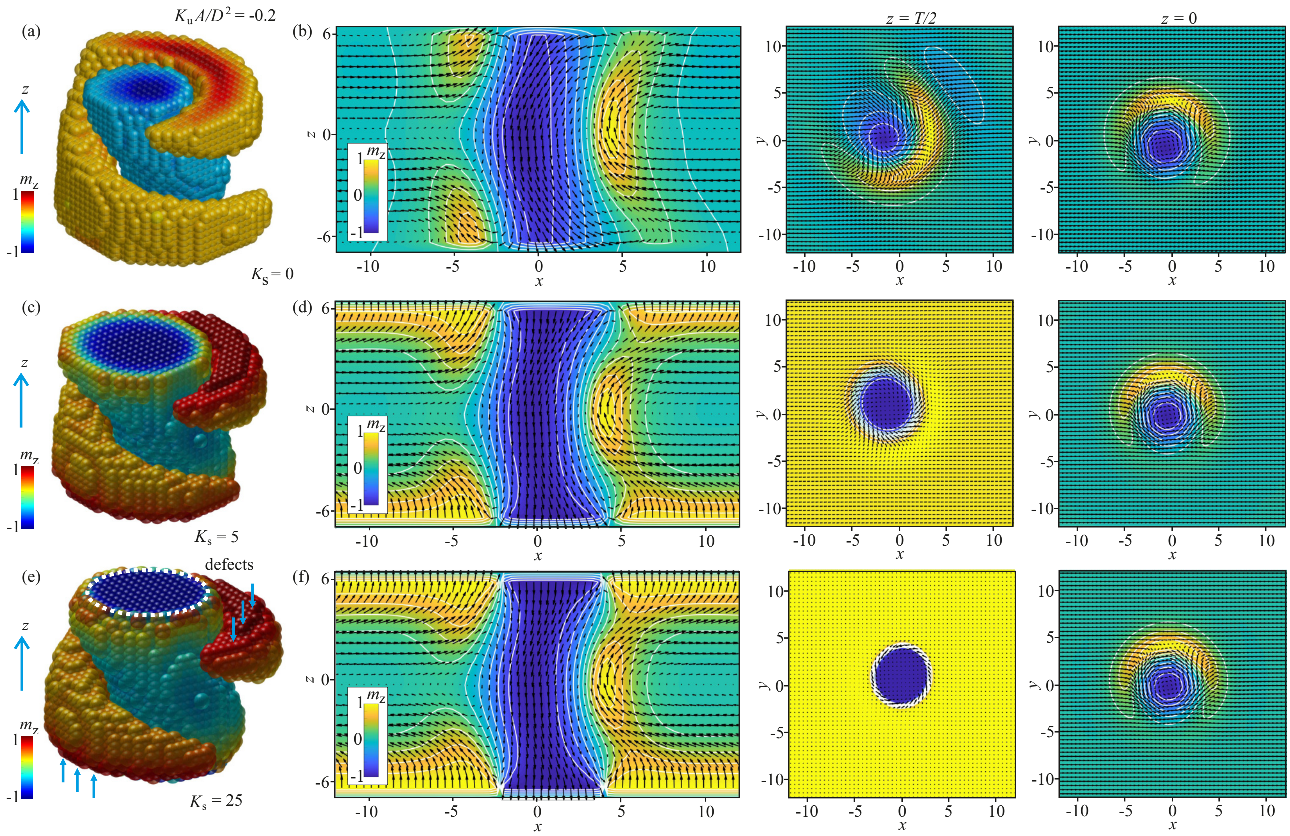

FIG. 2. Internal structure of isolated skyrmions subjected to increasing homeotropic anchoring $K_s > 0$: $K_sA/D^2 = 0$ (a), 5 (c), and 25 (e). The structure of isolated skyrmions is represented as color plots of m_z (b), (d), and (f) in the plane xz (first column) and in the xy cross sections at the surface (second column) and in the middle of the layer (third column). Skyrmion profiles in the middle of the layer remain visually unchanged, whereas the profiles at the surface acquire axisymmetric shape. Projections of the magnetization onto the corresponding plane are indicated with black arrows. The three-dimensional constructs with excluded spins of the conical phase are shown in (a), (c), and (e) for three values of the surface anchoring and fixed value of the bulk anisotropy $K_uA/D^2 = -0.2$. In (e), a ring of formed defects is shown by the white dashed line. Blue arrows indicate that the red coil associated with the domain boundary between isolated skyrmions and a conical state is squeezed into the interior of the layer. The internal structure of isolated skyrmions implies anisotropic character of their interaction (see text for details).

along particular directions. Qualitatively, the attracting anisotropic nature of such a skyrmion-skyrmion interaction can be explained on the basis of the so-called skyrmion shell [52,53]—a domain wall region separating the skyrmion core from the cone phase. After averaging over the z coordinate, the energy density of an isolated skyrmion on the plane xy can be characterized by characteristic lengths R_1 and R_2 that indicate several distinct regions in the radial energy density profiles (see, e.g., Ref. [53] and Fig. 4 therein for details). Then the energy density pattern consists of the positive energy "bag" located in the skyrmion center ($\rho < R_1$) and encompassed by extended areas with negative energy density, where the DM coupling dominates [2]. Negative asymptotics of the radial energy densities [$\Delta e(\rho) < 0$ for $\rho \gg 1$] predetermine the *repulsive* intersoliton potential for axisymmetric skyrmions [2], as would be the case for ISs in Fig. 3(a). For nonaxisymmetric skyrmions [Figs. 2(a)–2(f)] the energy densities $\Delta e(\rho)$ are positive at large distances from the skyrmion center ($\rho > R_2$). These areas correspond to the aforementioned "shells" separating the skyrmion core from the cone phase. The positive energy density of the shell leads to the attractive interactions between nonaxisymmetric skyrmion [52]. In other words, the phenomenon of the skyrmion-skyrmion attractive interaction in the cone phase is explained by the excessive energy density of the asymmetric shell (compared to those in the skyrmion core and the cone phase) [52].

In thin films, however, with the thickness corresponding to a fractional number of spiral periods, ISs would rather develop an anisotropic interaction since the excess of energy in a shell becomes more pronounced along particular directions or even spans a finite range of angles. If the number of skyrmion loops [red coils surrounding skyrmions in Figs. 2(a), 2(c) and 2(e)] is slightly larger than an integer, then two skyrmions arrange along the line, which connects a skyrmion center and a point, where a skyrmionic coil starts a new loop. If, on the contrary, the number of skyrmion coils is slightly smaller than an integer, the interskyrmion potential is almost isotropic. In this respect, three skyrmions may form two energetically different configurations: a skyrmion chain (lower energy) and a skyrmion cluster with skyrmions in the vertices of a triangle (higher energy). In both configurations skyrmionic clusters reduce their energy as compared with isolated entities, but apparently a potential barrier must be overcome to implement a transition between them (which will be computed elsewhere).

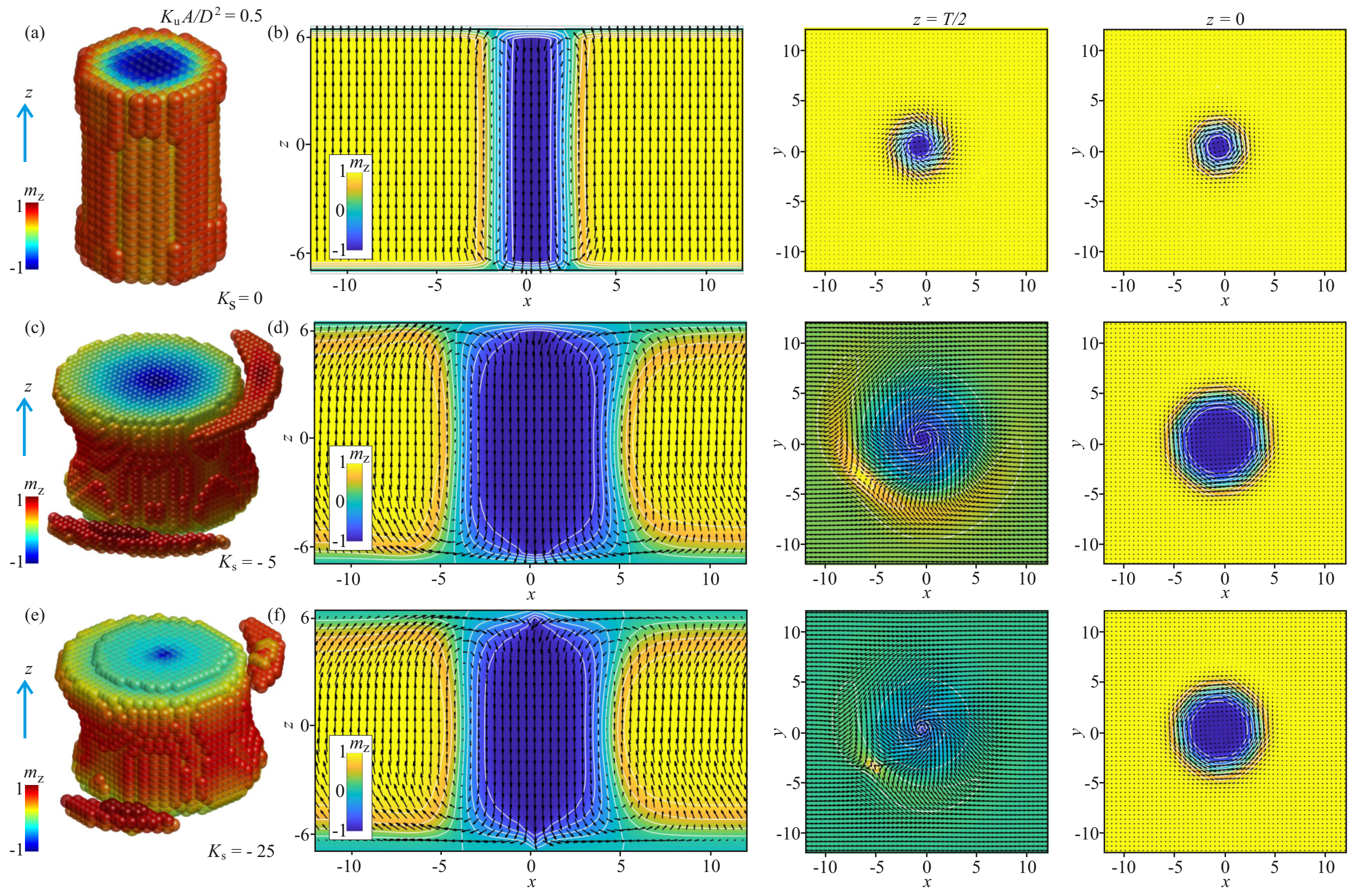

FIG. 3. Internal structure of isolated skyrmions subjected to increasing planar anchoring $K_s < 0$. The structure of isolated skyrmions is represented as color plots of m_z (b), (d), and (f) in the plane xz (first column) and in the xy cross sections in the middle of the layer (second column) and at the surface (third column). Whereas the central profiles retain their axisymmetric shape, the surface profiles become pronouncedly nonaxisymmetric. Projections of the magnetization onto the corresponding plane are indicated with black arrows. The three-dimensional constructs with excluded spins of the conical phase are shown in (a), (c), and (e) for three values of the surface anchoring and fixed value of the bulk anisotropy $K_uA/D^2 = 0.5$. Crescents formed only near the confining surfaces imply an anisotropic character of skyrmion interaction with two possible configurations within the skyrmion chains (see text for details).

Recently, such a tendency to form skyrmion chains has been demonstrated in CLCs with the thickness slightly larger than the spiral pitch, thus proving the 2D character of the skyrmion-skyrmion interaction [29,32]. Moreover, by using ambient-intensity unstructured light, the authors demonstrated large-scale multifaceted reconfigurations of skyrmion clusters (called skyrmion "crowds") into single-file lines or chains. Attraction of magnetic skyrmions mediated by the conical phase has been observed experimentally in thin (70 nm) single-crystal samples of Cu_2OSeO_3 taken using transmission electron microscopy [53]. In all of the videos recorded in Ref. [53], however, the skyrmions were in constant motion caused by the specimen charging under the electron beam, and different cluster configurations except skyrmion chains have been detected including even a squarelike arrangement of skyrmions [as shown by a snapshot of Fig. 2(a) in Ref. [53]]. Such a motion, although at a smaller scale, can be a result of frustration, when the constituent skyrmions attempt to minimize the anisotropic interskyrmion attraction.

Direct evidence of the field-dependent character of the interaction between individual magnetic skyrmions as well as between skyrmions and edges in B20-type FeGe nanostripes was also reported in Ref. [54]. Skyrmion clusters were observed by means of high-resolution Lorentz transmission electron microscopy. It was shown that above certain critical values of an external magnetic field the character of a long-range skyrmion interaction changed from attraction to repulsion. Such a behavior demonstrated a quantitative agreement with the results of micromagnetic simulations [55].

B. Attracting skyrmions specify the angular phase of the conical phase

I also notice that the structure of an isolated skyrmion reveals the phase of the conical state ψ_c (9), since the rotation in the conical phase is directly related to the formation of skyrmion coils. For example, from the location of the skyrmion crescent at the surface [Figs. 3(c) and 3(e)], one can deduce the in-plane component of the magnetization in the conical state. Such an insight becomes especially valuable in Lorentz transmission electron microscopy (LTEM) investigations of thin films or wedges of cubic helimagnets. Indeed, the electron microscopy shows featureless images for both the cone and saturated phases so one cannot directly confirm that

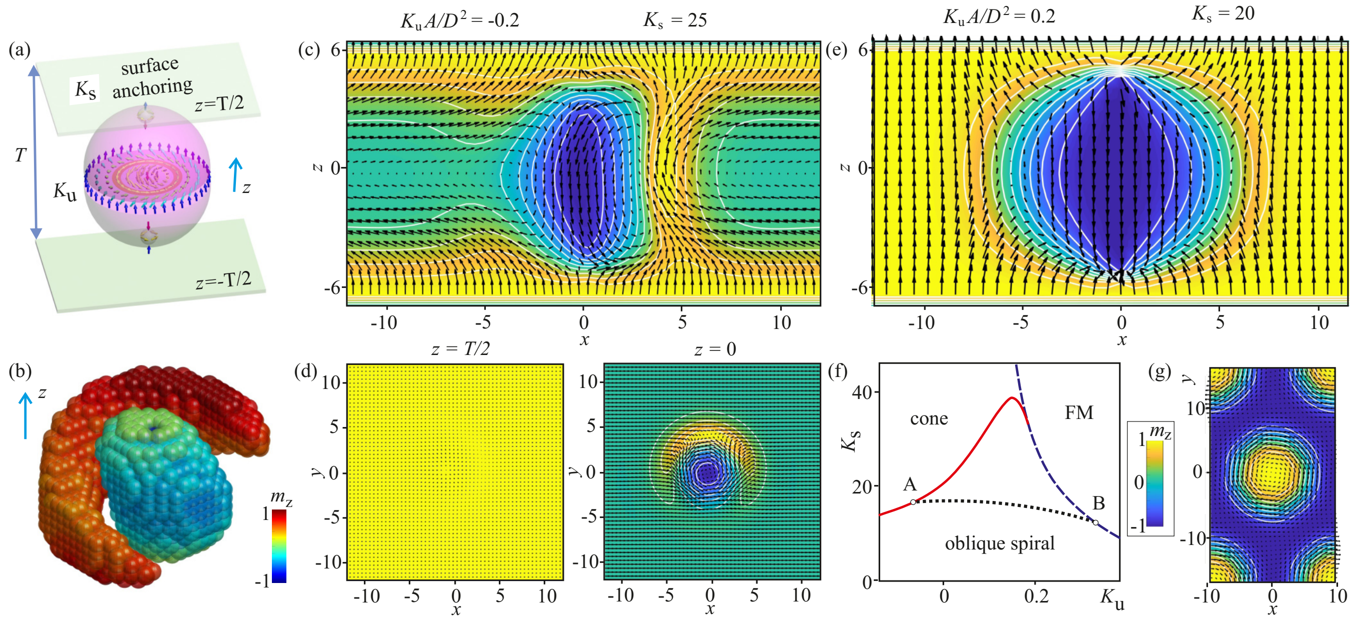

FIG. 4. (a) Schematic representation of torons—spatially localized three-dimensional skyrmions composed of a skyrmion filament of finite length cupped by two point defects terminating its prolongation. According to the 3D model in (b), torons are composed of a globulelike (blue) core centered around the magnetization opposite to the field and a fragment of a (red) coil with the magnetization along the field. Color plots of the magnetization component m_z exhibit the structure of an isolated toron in different crosscuts (c) and (d). Whereas in the middle of the layer [second panel in (d)], the magnetization distribution is similar to that of an isolated skyrmion [see, e.g., for comparison Fig. 2(b), third panel], the spins at the surface are all magnetized homogeneously along z [first panel in (d)]. The internal structure of constituent torons within the toron lattice is shown in (e) and (g). Above the dotted line A–B (f), such a lattice is energetically more favorable as compared with the skyrmion lattice (see text for details).

featureless regions of experimental images are, e.g., the cone phase [53,56]. One can, however, identify the conical phase owing to the skyrmion attraction (otherwise, skyrmions would repulse in the homogeneous state), and moreover deduce its phase from the skyrmionic pattern.

From Fig. 3(c), it becomes evident that the crescent at the lower surface does not correlate with the crescent at the upper surface, which is valid while the edge conical states are localized near the surfaces and do not intersect in the middle of the layer, which is the case far from the line b–f within the region 3 of the phase diagram [Fig. 1(a)]. Two interacting skyrmions, however, prefer to align along the line going through their centers and the centers of their crescents. This phenomenon was deduced in Refs. [57–59] for 2D skyrmions in polar magnets with easy-plane anisotropy. It was shown that, in the head-to-head configuration, 2D skyrmions form pairs with a fixed interskyrmion distance, implying the attractive nature of their interaction. The calculated interskyrmion potential for the side-by-side configuration reveals the repulsive character of skyrmion-skyrmion interaction at large distances. Thus I expect that the same logic would hold for quasi-2D skyrmions in Figs. 3(c) and 3(e). One can envision two energetically degenerate configurations of such a skyrmion pair, in which the crescents of one skyrmion are located either on the same side with respect to the skyrmion core or on the opposite sides. In any case, a pair of interacting skyrmions adapts the surrounding conical phase to reach the minimum of the interskyrmion potential. Moreover, these skyrmions are also expected to form one-dimensional chains running along the canted magnetization at the surface.

V. TORONS AS AN ENERGETICALLY FAVORABLE SUBSTITUTE OF SKYRMIONS

For ISs with $K_u < 0$ [Figs. 2(a)–2(f)] as well as for $K_u > 0$ (not shown), the homeotropic surface anchoring ($K_s > 0$) in the first place compresses the magnetization distributions at the surfaces and eventually results in a ring of energy-costly defects [compare profiles in the second row of Figs. 2(b), 2(d) and 2(f)]. Skyrmion profiles in the middle of the layer remain virtually unchanged [compare profiles in the third row of Figs. 2(b), 2(d) and 2(f)]. The red coil "sinks" deep into the layer [shown by blue arrows in Fig. 2(e)]. Such an incompatibility with the surrounding state and the associated energy cost due to formed defects encourages one to consider another skyrmion-based particle—a toron (Fig. 4).

Toron [4,39,60,61] represents a localized particle consisting of two Bloch points at finite distance and a convex-shaped skyrmion stretching between them [Fig. 4(a)]. The central magnetization distribution [Fig. 4(d)] is similar to that of an IS [third column in Figs. 2(b), 2(d) and 2(f)], whereas the surface profiles are the saturated states [Fig. 4(d)]. Due to the gradually varying skyrmion helicity, the energy density becomes negative in the toron's cross section, which is balanced by the positive energy contributions from two Bloch points (see for details, e.g., Refs. [60,61]). Helicity here is defined as the angle γ, which enters the formula $\psi = Q\phi + \gamma$. To describe skyrmionic states, one usually uses spherical coordinates for the magnetization (4) and cylindrical coordinates (ρ, ϕ) for the spatial variable. Thus such a particle as a toron utilizes energetically favorable additional twists due to LI $\mathcal{L}^{(z)}_{x,y}$, as

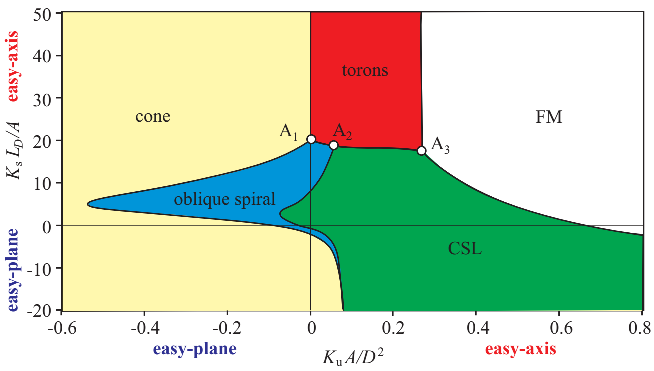

FIG. 5. Phase diagram of states in the space of control parameters (K_u, K_s). The regions of the thermodynamical stability are colored by red (hexagonal lattice of torons), yellow (cones), green (helicoids), blue (oblique spiral state), and white (ferromagnetic state). The detailed description of the phase transitions between modulated phases is given in the text.

described in Sec. VIII, and simultaneously satisfies the boundary conditions at the confining substrates with strong surface anchoring, which makes it an energetically more favorable particle as compared with a skyrmion in a range of control parameters. The transition between skyrmions and torons has been recently observed [39] to occur via so called toron or skyrmion hybrid structure—a particle with a point defect near one surface (like in a toron) and a ring of defects near the other surface (like in a skyrmion). The energy barriers for such a process calculated with the geodesic nudged elastic band method will be published elsewhere.

From the corresponding 3D model [Fig. 4(b)], it follows that the torons also develop an attracting anisotropic interaction as was discussed for ISs in Sec. IV A. According to numerical simulations, the lattice of torons (TL) [Figs. 4(e) and 4(g)] replaces the SkL at the line A–B of the phase diagram [Fig. 5(f)], i.e., for higher values of the homeotropic anchoring K_s. Moreover, with the simultaneous effect of the easy-axis bulk and easy-axis surface anisotropies, TL becomes a thermodynamically stable state. In the phase diagram (Fig. 5), the region of TL stability is shown by the red-shaded region. Interestingly, there is no upper boundary for such a region. The reason is the same as already discussed for the conical phase: once the spins at the confining surfaces are aligned by the surface anchoring [e.g., for the conical phase above the line b–e in the region 1 of Fig. 1(a)], the core structure in the middle of the layer does not change. The line A_1–A_2–A_3 in Fig. 5, which signifies the first-order phase transition with respect to one-dimensional spirals, lies a bit higher than the line A–B in Fig. 4(f), which merely represents the computed transition between metastable SkL and the lattice of torons. At the line A_1–A_2, TL undergoes a first-order phase transition with the one-dimensional oblique spiral state, whereas at the line A_2–A_3 it is with the one-dimensional helicoid.

Surface profiles for skyrmions with planar anchoring $K_s < 0$ and, e.g., easy-axis bulk anisotropy K_u [Figs. 3(c)–3(f)], on the contrary, reduce to two point defects centered at the crescent and skyrmion core [Fig. 3(f), second panel], whereas the central profiles retain their axisymmetric shape [third row in Figs. 3(b), 3(d) and 3(f)]. Obviously, torons cannot provide any energetic alternative to SkLs.

VI. PHASE DIAGRAM OF STATES IN THIN LAYERS OF CLCs

At the phase diagram (Fig. 5), the helicoid [also called a chiral soliton lattice (CSL)] occupies the green-shaded area. The wave vector of CSL is directed within the plane xy (for definiteness, along y axis). For zero anisotropy values, such spirals have lower energy as compared with the conical state, which is readily explained by the additional surface twists in thin-film nanosystems, i.e., owing to the same LIs $\mathcal{L}^{(z)}_{x,y}$, which also underlie skyrmion stability. In the same way, whereas the LIs with the derivatives along the axes x and y govern the magnetization rotation in spiral states, the LI with the derivative along z leads to the gradual change of the spiral helicity towards upper and lower surfaces with the penetration depth $4\pi L_D/10$. This effect accumulates additional negative energy compared with the cones not decorated by the additional surface twists [56,62]. Hence the CSL is stabilized in some range of anisotropic contributions [56,63] and is the main modulated state for the easy-plane anchoring K_s (which supports in-plane magnetization rotation at the surfaces) and easy-axis bulk anisotropy K_u (which supports magnetization rotation in the plane xz in the middle of the layer).

The CSL transforms into the FM state only at the line A–B [Fig. 6(a)]. In this case, the spiral profiles in the middle of the layer dominate and overcome the effect of the homeotropic anchoring to pin the spins at the surface and to "freeze" the whole structure in the middle of the layer, as was considered for cones and torons. Above the line A–B for a sufficiently high anchoring, the spiral represents a system of isolated noninteracting domain walls (DW). Such DWs contain disclination lines running along the surface and separate domains with the magnetization along and opposite to the z axis [Fig. 6, third panel in (c)]. Such a spiral expansion is similar to the process of a field-driven CSL expansion in bulk helimagnets with the critical field (8) although being defect free: while the polar angle in the spiral state retains its constant value $\pi/2$, the azimuthal angle is expressed as a set of elliptical functions; as derived by Dzyaloshinskii within phenomenological theory, the solutions for this field-distorted spiral are obtained from the well-known differential equations for the nonlinear pendulum. Recently, such an expansion of the chiral magnetic soliton lattice has been observed by Lorenz microscopy and small-angle electron diffraction [64] in the chiral helimagnet $Cr_{1/3}NbS_2$.

Along the line C–D, the CSL transforms into the conical state. Since it is the first-order phase transition, it must be accompanied by the coexisting domains of both phases, which are readily resolved experimentally by Lorentz transmission electron microscopy investigations in thin layers of cubic helimagnets, e.g., in FeGe [56].

In the vast region between the lines D–E–F and D–G–F, the transition between CSL and cones occurs via an intermediate oblique spiral state, which originates from the interplay between the surface twists and the anisotropies K_s and K_u [65]: whereas the negative energy associated with the surface

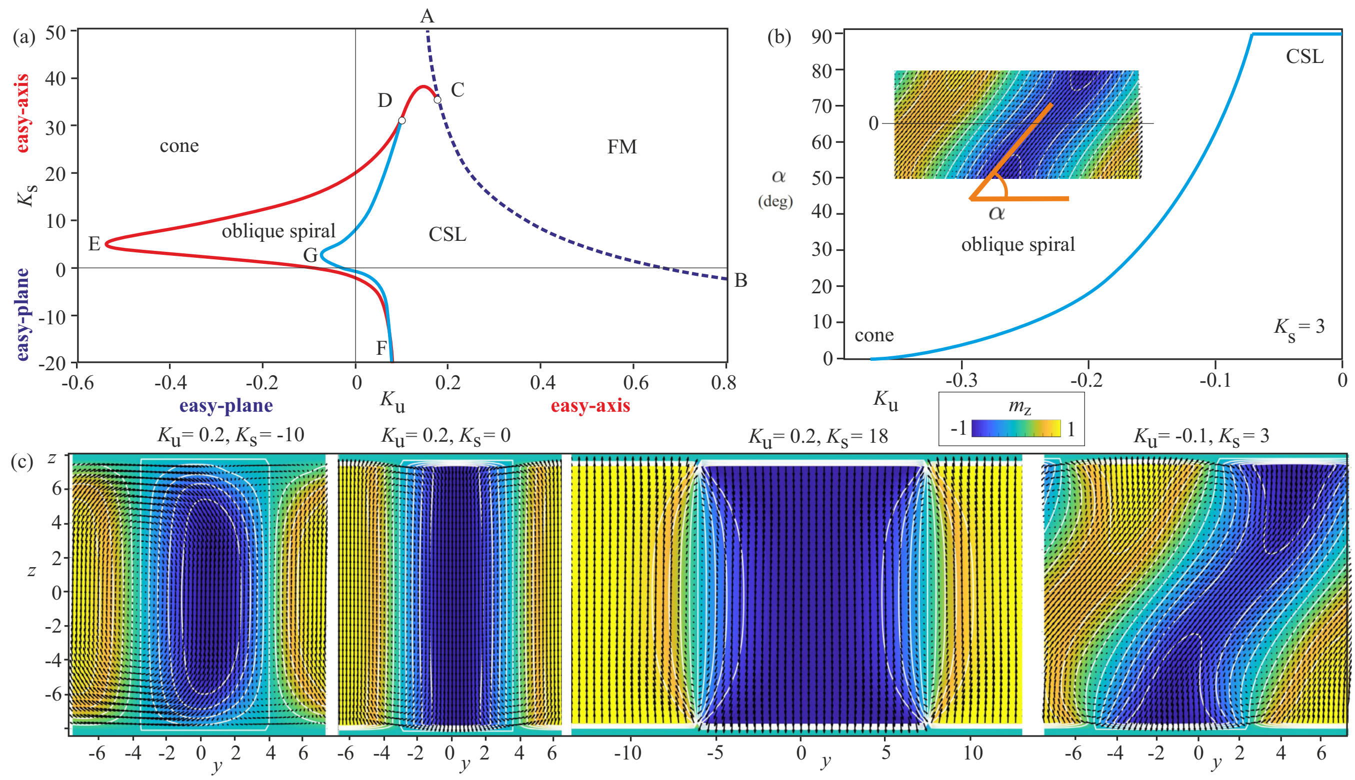

FIG. 6. (a) Diagram of 1D solutions for model (4) in the space of control parameters (K_u-K_s) for the fixed value of the thickness, $T = 4\pi L_D$. The color plots in (c) stand for m_z components of the magnetization. m_y and m_z components are shown with thin black arrows. The straight spiral state [also called a chiral soliton lattice (CSL)] expands into a system of isolated solitons [third panel in (c)] only along the line A–B. Additionally, the strong surface anchoring leads to a formation of defects near the confining surfaces. Otherwise, the CSL transforms into the conical state: such a transition may occur either as the first-order phase transition along the line D–C or via an intermediate oblique spiral state [fourth panel in (c)] along the line D–G–F. Then, in the latter case, the tilt angle α (b) smoothly decreases from the value $\pi/2$ in the CSL state to the value $\alpha = 0$ in the conical state. A procedure to determine a canting angle α for an oblique spiral state is shown as an inset in (b) (see also text for details).

twists remains almost unchanged, the canting leads to the lowering of the positive easy-plane anisotropy energy K_u. To introduce a procedure for defining a canting angle, I notice that an oblique spiral represents a combination of a flat spiral in the middle of the layer and a roundish part near the surfaces related to the chiral surface twists [Fig. 6, third panel in (c)]. Therefore, I consider two profiles of the m_y components of the magnetization located at some fixed distance b from each other near the layer middle [Fig. 6, inset in (b)]. In this undistorted part of an oblique spiral, these profiles are essentially the same but acquire a phase shift with respect to each other [65]; a is the distance between, e.g., the neighboring minima of m_y profiles. Thus the canting angle can be introduced as $\tan\alpha = b/a$. For a straight CSL state, $\alpha = 90^\circ$, and for a conical state, $\alpha = 0$. As shown by Fig. 6(b), the angle of canting α for $K_s = 3$ and variable K_u monotonically decreases with the growing UA and thus signifies transition into the conical phase at the line D–E–F.

Since in CLC an electric field fulfills the role of K_u and hence is often used to switch between different textures, the considered transition can be easily devised experimentally. Interestingly, being unidentified in experiments on thin layers of chiral helimagnets (although predicted theoretically in Ref. [65] for epitaxial films of MnSi), oblique spirals are known in CLCs under the name of "nonsingular fingers of CF1 type" [19,66]. In Ref. [66] in particular, a periodic finger pattern composed of CF1s was experimentally shown to transform into a conical state [called translationally invariant configuration (TIC) with uniform in-plane twist $\theta_c \approx \pi/2$ because of the weak in-plane anchoring]. The fingers gradually widened and then merged in order to form the modulated TIC.

VII. 3D SKYRMION DROPLETS AS A DOMAIN BOUNDARY BETWEEN TWO TYPES OF THE CONICAL STATE

In addition to the conical state with the positive values of the polar angle, $\theta_c(z) \in [0, \pi/2]$, one may also encounter its higher-energy counterpart [Fig. 7(a)], in which the polar angle sweeps the whole diapason $\theta_c \in [-\pi/2, \pi/2]$, i.e., the magnetization rotates from the state opposite to the z axis at the lower surface to the state along z at the upper surface. Although such a state emerges as a metastable solution in the whole range of control parameters for the fixed layer thickness $T = 4\pi L_D$, I expect that the energy difference between the two conical states becomes negligibly small with the increasing film thickness; i.e., if the central part with the planar magnetization $\theta_c(z = 0) = \pi/2$ [Fig. 7(b)] becomes wider and does not allow

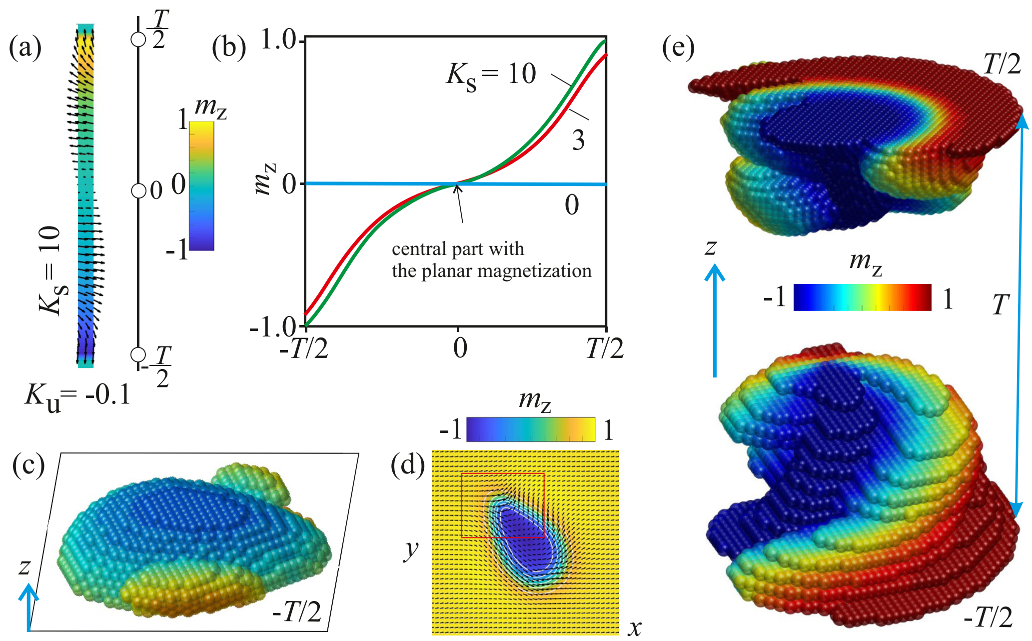

FIG. 7. Internal structure of a metastable conical state arising due to the homeotropic anchoring. The color plot in (a) exhibits m_z component; black arrows show projection of the magnetization onto the xz plane. Magnetization profiles plotted for several values of K_s in (b) demonstrate the full cycle of spin rotation from the state down at the lower surface to the state up at the upper surface. Interestingly, the domain boundary between two conical states reduces to the so called droplet—a topologically trivial particle with zero topological charge $Q = 0$. The 3D model of such a droplet is shown in (c) and the magnetization distribution in the xy plane in (d). For completeness, I also construct 3D models for so called chiral bobbers localized near layer surfaces and culminating in two point defects (e). I notice that the metastable conical state (a), which may actually acquire the same energy as the cone in region 2 of Fig. 1(a) with the increasing film thickness, would accommodate chiral bobbers with opposite polarities (see text for details).

intersection of surface states, the bulk and surface anisotropies would have no preferences as for the realized conical state.

Interestingly, the domain boundary between two conical states transforms into a 3D skyrmion droplet [Figs. 7(c) and 7(d)] confined near the surfaces [67]. In this sense, such a droplet reminds one of a chiral bobber [68], the internal structure of which is balanced by the negative energy contribution from additional surface twists due to $\mathcal{L}^{(z)}_{x,y}$ and the positive energy due to the point defect [60]. The 3D model of such a bobber within the conical state is shown in Fig. 7(e). I note that the bobbers within the second conical state would have opposite polarities at both surfaces, which would extend functionalities of bobber-based spintronic devices.

Droplets are topologically trivial states with $Q = 0$. The magnetization distribution at the lower surface shows that they have skyrmion and antiskyrmion parts with the former occupying a larger area [67]. Such skyrmion droplets also may be considered as nuclei of a spiral state if going from the region of cone stability into the region with the CSL. In the same way, isolated skyrmions within the homogeneous state undergo elliptical instability and stretch into a spiral domain that has lower energy as compared with the saturated one [25]. Two-dimensional analogs of skyrmion droplets have been studied in a number of papers [67,69]. Interestingly, the droplets are stabilized not only owing to DMI or dipolar interactions, but also can be dynamically nucleated, sustained, and manipulated [69].

VIII. DISCUSSION: THE RISE OF MAGNETIC AND LIQUID-CRYSTAL SKYRMIONICS

A. From stable SkL in bulk cubic helimagnets to metastable skyrmions in spintronic devices

The study of magnetic skyrmions emerged from the search for stabilization mechanisms helping to overcome the constraint of the Hobart-Derrick theorem [10]. Hobart and Derrick found with general arguments that multidimensional localized states are unstable in many physical field models. Inhomogeneous states may appear only as dynamic excitations, but static configurations collapse spontaneously into topological singularities. As a consequence, the solutions of corresponding nonlinear field equations are restricted to one-dimensional solitons and such localized structures as magnetic skyrmions are not expected to exist.

In this search, one managed not to become deceived by magnetic bubbles [70], which represent circular domains with the magnetization antiparallel to the homogeneously magnetized state and thin domain walls as transition regions between the two magnetization orientations. In spite of the topological similarity between skyrmions and common bubbles (indeed, the skyrmion may be naively visualized as a bubble without its core), they are different branches of solutions of micromagnetic equations. Bubble domains arise only as a result of the surface depolarization and the tension of ordinary domain walls and are intrinsically unstable. This fact, however, does not impede nowadays calling magnetic bubbles skyrmions.

Existence of chiral skyrmions in magnetism was predicted and investigated theoretically by Bogdanov, Yablonsky, and Hubert starting in 1989 and subsequent works [1,2]. They identified a group of low-symmetry magnetic materials with broken inversion symmetry that defy skyrmion instability. As discussed in the Introduction, magnetic interactions imposed by the handedness of the crystal structure [DMI (1)] provide a cherished stabilization mechanism. Investigations of such chiral magnetic skyrmions, however, for a long time have been restricted to theoretical studies and skyrmions were even hailed as some exotic elusive objects, which is partially related to the inability of experimental techniques to identify nanoscale particles.

An intensive experimental search for magnetic skyrmions commenced two decades after their theoretical prediction in bulk helimagnets with a cubic chiral B20 structure like MnSi and FeGe [13]. Long-term experimental investigations of the chiral helimagnet MnSi [71,72], which is considered to be the most investigated chiral helimagnet—the "toy tool" of the chiral magnetism—reported numerous physical anomalies along the magnetic ordering transition and, particularly, indicated the existence of a small closed area in the (H, T) phase diagram, the so-called "A phase." However, only in 2009 by the group of Pfleiderer [13] was a complex multidimensional character of chiral modulated magnetic states within the A-phase pocket associated with skyrmions. On one hand, the small size of a region at the phase diagram, where skyrmions were rendered into a thermodynamically stable hexagonal skyrmion lattice (SkL), was discouraging and skyrmions were thought to be only responsible for experimentally observed precursor effects near the ordering temperatures [73]. On the other hand, however, the A-phase region posed the question of thermodynamical stability of skyrmions. The quest for stabilization mechanisms showed that, within an isotropic phenomenological model, the skyrmion lattice is always a metastable solution. However, the energetic difference to its main competitor, the conical phase, is weak and reduces to a minimum for those magnetic fields that stabilize the A phase [24]. As a consequence, weak interactions such as the softening of the magnetization modulus [37], dipolar interactions, fluctuations [13,74], etc., may modify the energetic landscape and eventually stabilize the SkL in the A-phase pocket. Due to this subtle energetic balance, the boundaries of the A phase can be changed substantially by relatively small external stimuli, such as pressure [75] or electric fields [76–79]. Recent experimental findings also revealed a vast area of low-temperature skyrmion stability in the bulk insulating cubic helimagnet Cu_2OSeO_3, when the magnetic field is applied along the easy $\langle 001\rangle$ crystallographic axis, thus identifying the crucial role of cubic and exchange anisotropies [80,81].

The first direct observations of SkLs in nanolayers of cubic helimagnets $(Fe_{0.5}Co_{0.5})Si$ [82] and FeGe [83] demonstrated that the internal structure of chiral skyrmions, being modulated by additional surface twists, also leads to their thermodynamical stability even without any anisotropic contributions [49,50,56,62]. Indeed, in bulk cubic helimagnets, only the Lifshitz invariants $\mathcal{L}_{x,y}^{(x,y)}$ govern the magnetization rotation in skyrmions. These LIs fix the skyrmion helicity at the value $\gamma = \pi/2$ (Bloch-like fashion of rotation). In magnetic nanolayers on the contrary, the LI $\mathcal{L}_{x,y}^{(z)}$ with the magnetization derivative along z comes into play. This is the energy term that stipulates the magnetization rotation within the conical phase as well. For skyrmions, $\mathcal{L}_{x,y}^{(z)}$ leads to the gradual change of the skyrmion helicity $[\gamma = \pi/2 \pm \xi(z)]$ towards upper and lower surfaces with the penetration depth $4\pi L_D/10$ [56,62]. This effect accumulates additional negative energy compared with the cones not decorated by the surface twists [56,62]. Hence SkL is stabilized in a broad range of applied out-of-plane magnetic fields and nanolayer thicknesses T (up to the confinement ratio $\nu = T/4\pi L_D \approx 8$). ISs within the conical phase, however, are metastable particles for all values of the confinement ratio [52,60] (except the small region for $\nu \leqslant 1$ in which the energy of an IS becomes negative). The reason lies in the specific transient region between an IS and the conical phase (dubbed "shell" in Ref. [52]) that bears the positive energy density and increases linearly with the thickness. Moreover, the additional surface twist (and hence an associated negative energy) is essentially reduced in IS as compared with SkL [52,60,63]. Still, an applied out-of-plane magnetic field is considered as a crucial ingredient for both bulk and thin-film chiral magnets to stabilize a hexagonal skyrmion order [24].

For applications in magnetic data storage technologies and in the emerging spin electronics, the isolated skyrmions are more preferable, since they represent metastable particles within the conical or the homogeneous states [25,52]. Such localized skyrmionic excitations may be controlled and manipulated [84] and, therefore, may find application in spintronic devices. Skyrmionic "particles" may be also driven together to form complex noncollinear magnetic textures—skyrmion lattices. The formation of the lattice is determined by the stability of the localized solitonic cores and their geometrical incompatibility that frustrates homogeneous space filling. However, if the formation of skyrmion lattices is suppressed, isolated skyrmions continue to exist until they elongate and expand into a band with helicoidal modulation and eventually fill the whole space. Below the critical "strip-out" field, the spiral state represents the minimum with lower energy as compared to the local minima with the metastable isolated skyrmions. Therefore, one usually avoids the regions of phase diagrams where the energy of an IS becomes negative and thus stipulates the formation of SkL. Still, creating patterns from metastable solitonic units poses the question of mutual interactions, in particular at high densities.

Axisymmetric skyrmions exist as ensembles of weakly repulsive particles in the saturated phase of noncentrosymmetric magnets [25,85], in which all the atomic spins are parallel to an applied magnetic field, which is strong enough to saturate all the modulated states. Axisymmetric chiral skyrmions may also exist in systems with strong easy-axis anisotropy, potentially even at zero field. The detailed evolution of isolated skyrmions from the strip out at low fields to the collapse at high fields has been reported in PdFe/Ir(111) bilayers with the induced DMI and a relatively high value of the uniaxial anisotropy [85,86]. On the other hand, being embedded in the cone phase of chiral ferromagnets, isolated skyrmions acquire a nonaxisymmetric shape, become mutually attractive, and so tend to produce skyrmion clusters [52]. Thus, generically, the character of skyrmion-skyrmion interaction as well as their internal structure are shaped by a surrounding "parental" state. In the skyrmion racetrack [16,87,88]—a prominent model for future information technology—information flow is encoded in the isolated skyrmions [17] moving within a narrow strip. Then, the knowledge of skyrmion characteristics allows one to foresee the skyrmion behavior in spintronic devices. Indeed, the ISs may run along the side boundaries of racetracks being attracted by the edge states with the complex spin structure in the conical state. Alternatively, skyrmions may become repelled by the flat edge states formed within the homogeneous state [89].

B. Chiral liquid crystals as model systems for probing behavior of skyrmions

In CLCs, a rich variety of 2D and 3D localized structures such as cholesteric bubbles (spherulitic domains) [90,91], cholesteric fingers [66], torons [92], and other specific solitonic textures [93] have been observed during the past four decades. In contrast to magnetic systems favoring smooth distributions of the order parameter, liquid crystals usually form patterns composed of various types of singularities. Defects in liquid crystals are of various dimensionalities, not only point defects but also the line and walls, and appear due to the prevalence of orientational order over positional order in the applied magnetic or electric fields. Thus the CLC skyrmionics commenced rather from the classification and resolution of an internal structure of versatile particlelike states emerging due to strong boundary conditions incompatible with the favored twist. In this sense, elastic constant anisotropy and confinement (surface anisotropy) provide alternative routes [39] to overcome the constraints of the Derrick-Hobbart theorem [10]. Consequently, CLCs are ordinarily modeled within the Landau–de Gennes theory in terms of the tensor order parameter [19,22], which encompasses the full degree of the order and orientation in CLCs. A comprehensive comparative study of tensor-based CLCs and vector-based ChMs theoretical models have been performed in Ref. [22] with a number of important conclusions. In particular, a decisive role of an applied magnetic field in the stability of magnetic skyrmions was underlined. A square lattice of merons was shown to include disclination lines in CLCs [22], which are treated as the regions with the suppressed magnitude of the magnetization in ChMs [12]. Such a "softening" of the magnetization occurs via the energy terms in the Landau expansion for small values of the magnetization and includes only even powers related to reversal in the sign of the magnetization (only for even powers of $\mathbf{M}$ is time reversal symmetry preserved). From numerical investigations on 2D models of isotropic chiral ferromagnets, such a staggered half-skyrmion square lattice at zero field of the phase diagram near the transition temperature appears through a rare case of an instability-type nucleation transition [12] and is thought to be responsible for observed precursor anomalies [73]. For lower temperatures, however, nonuniform magnetic states include only rotation of $\mathbf{M}$ without any change in its magnitude. For CLCs, the bulk free energy within the Landau–de Gennes theory includes also cubic energy terms [22]. Interestingly, a square lattice of vortices and antivortices with topological charges $Q = \pm 1/2$ (alternatively called a meron cluster) can be stabilized in frustrated magnets with competing exchange interactions. Such a state does not face the problem of defects, since the skyrmion helicity as well as the sign of the topological charge are arbitrary [94].

The simpler Frank-Oseen model used in the present manuscript has its own merits and can translate insights between CLCs and ChMs communities. Indeed, the role of mentioned surface twists in the stability of magnetic skyrmions in thin-layered samples has been investigated theoretically [62] and experimentally [48,56] since 2013. Reference [23], however, unintentionally overlooked those findings and developed a theory of CLC skyrmion states with varying azimuth. Thus, to avoid any unintended reproduction of known results, one should bridge the gap between the CLC and ChM communities and concertedly address the topological phases realized in both condensed-matter systems. Presently, chiral liquid crystals are deservedly considered as an ideal model system for probing behavior of different modulated structures on the mesoscopic scale [4] due to much more developed experimental techniques. And, in particular, it was shown that different regimes of skyrmion interaction (i.e., mentioned interskyrmion attraction and/or repulsion) can be achieved by an analog of the conical phase with variable polar angle [95].

IX. CONCLUSIONS

To conclude, I have demonstrated the effect of surface anchoring on the internal structure and properties of isolated skyrmions and torons based on numerical minimization of the free-energy functional. I found that depending on the control parameters (bulk and surface anisotropies) the conical phase is uniquely modulated across the film thickness and thus hosts isolated skyrmions or torons with a distinct internal structure. Isolated skyrmions are argued to develop an anisotropic skyrmion-skyrmion interaction, which is dominated either by the skyrmion profiles in the middle of the layer (Fig. 2) or by the profiles near the confining surfaces (Fig. 3). In either case, skyrmions form energetically favorable chains as an alternative to skyrmion clusters with the hexagonal arrangement of constituent particles. In the limit of strong homeotropic anchoring, torons (Fig. 4) were shown to gain the thermodynamical stability in a vast area of the constructed phase diagram (Fig. 5). The mechanism of toron stability owing to the combined effect of easy-axis bulk and surface anisotropies is reminiscent of the SkL stability in an applied magnetic field in cubic helimagnets. The constructed phase diagram was also shown to contain one-dimensional straight and oblique spiral states (Fig. 6) that undergo first- and second-order phase transitions with the conical state. Just like the spiral solutions obtained within the Dzyaloshinskii theory, the spirals in CLCs may expand and release isolated solitons or alternatively they may become "frozen" by the surface anchoring with almost unchanged internal structure. Skyrmion droplets (Fig. 7)—topologically trivial particles—were in addition considered from a different perspective as a domain boundary between the conical states with different internal structure. Thus I emphasize that the control over the skyrmion structure provided by the applied magnetic field in chiral magnets can be substituted by the interplay of confinement and anchoring bringing about potential soliton-based information displays and other technologies. Moreover, since the surface- or interface-induced interactions (e.g., the Dzyaloshinskii-Moriya interaction and the surface or interfacial anisotropy) emerge in chiral magnets, the way of engineering the skyrmion properties by means of the surface anchoring is applicable for both condensed-matter systems.

ACKNOWLEDGMENTS

The author is grateful to I. Smalyukh, U. Rößler, K. Pappas, V. Uzdin, I. Tambovtcev, and I. Lobanov for useful discussions. A.O.L. thanks U. Nitzsche for technical assistance and acknowledges JSPS Grant-in-Aid (C) No. 21K03406.

[1] A. N. Bogdanov and D. A. Yablonsky, Theormodynamically stable vortices in magnetically ordered crystals. Mixed state of magnetics, Zh. Eksp. Teor. Fiz. **95**, 178 (1989) [Sov. Phys. JETP **68**, 101 (1989)].

[2] A. Bogdanov and A. Hubert, Thermodynamically stable magnetic vortex states in magnetic crystals, J. Magn. Magn. Mater. **138**, 255 (1994); The stability of vortex-like structures in uniaxial ferromagnets, **195**, 182 (1999).

[3] N. Nagaosa and Y. Tokura, Topological properties and dynamics of magnetic skyrmions, Nat. Nanotechnol. **8**, 899 (2013).

[4] P. J. Ackerman and I. I. Smalyukh, Diversity of Knot Solitons in Liquid Crystals Manifested by Linking of Preimages in Torons and Hopfions, Phys. Rev. X **7**, 011006 (2017).

[5] I. I. Smalyukh, Review: knots and other new topological effects in liquid crystals and colloids, Rep. Prog. Phys. **83**, 106601 (2020).

[6] M. J. Ablowitz, *Nonlinear Dispersive Waves: Asymptotic Analysis and Solitons* (Cambridge University Press, Cambridge, UK, 2011).

[7] S. Tsesses, E. Ostrovsky, K. Cohen, B. Gjonaj, N. H. Lindner, and G. Bartal, Optical skyrmion lattice in evanescent electromagnetic fields, Science **361**, 993 (2018).

[8] I. Chuang, R. Durrer, N. Turok, and B. Yurke, Cosmology in the laboratory: Defect dynamics in liquid crystals, Science **251**, 1336 (1991).

[9] R. Rajaraman, *Solitons and Instantons: An Introduction to Solitons and Instantons in Quantum Field Theory* (North-Holland, Amsterdam, 1982).

[10] R. H. Hobart, On the instability of a class of unitary field models, Proc. Phys. Soc. London **82**, 201 (1963); G. H. Derrick, Comments on nonlinear wave equations as models for elementary particles, J. Math. Phys. **5**, 1252 (1964).

[11] T. H. R. Skyrme, Particle states of a quantized meson field, Proc. R. Soc. London, Ser. A **262**, 237 (1961).

[12] U. K. Rößler, A. N. Bogdanov, and C. Pfleiderer, Spontaneous skyrmion ground states in magnetic metals, Nature (London) **442**, 797 (2006).

[13] S. Mühlbauer, B. Binz, F. Jonietz, C. Pfleiderer, A. Rosch, A. Neubauer, R. Georgii, and P. Boni, Skyrmion lattice in a chiral magnet, Science **323**, 915 (2009).

[14] T. Moriya, Anisotropic Superexchange Interaction and Weak Ferromagnetism, Phys. Rev. **120**, 91 (1960).

[15] I. E. Dzyaloshinskii, Theory of helicoidal structures in antiferromagnets. I. Nonmetals, J. Sov. Phys. JETP-USSR **19**, 960 (1964); Theory of helicoidal structures in antiferromagnets. II. Metals, **20**, 223 (1965).

[16] E. M. R. Tomasello, R. Zivieri, L. Torres, M. Carpentieri, and G. Finocchio, A strategy for the design of skyrmion racetrack memories, Sci. Rep. **4**, 6784 (2014).

[17] A. Fert, V. Cros, and J. Sampaio, Skyrmions on the track, Nat. Nanotechnol. **8**, 152 (2013).

[18] Y. Huang, H. Chen, G. Tan, H. Tobata, S. Yamamoto, E. Okabe, Y. Lan, C. Tsai, and S. Wu, Optimized blue-phase liquid crystal for field-sequential-color displays, Opt. Mater. Express **7**, 641 (2017).

[19] P. Oswald and P. Pieranski, *Nematic and Cholesteric Liquid Crystals: Concepts and Physical Properties Illustrated by Experiments* (CRC Press, Boca Raton, FL, 2005).

[20] M. Kleman and O. D. Lavrentovich, *Soft Matter Physics: An Introduction* (Springer-Verlag, New York, 2003).

[21] H. R. O. Sohn, P. J. Ackerman, T. J. Boyle, G. H. Sheetah, B. Fornberg, and I. I. Smalyukh, Dynamics of topological solitons, knotted streamlines, and transport of cargo in liquid crystals, Phys. Rev. E **97**, 052701 (2018).

[22] A. Duzgun, J. V. Selinger, and A. Saxena, Comparing skyrmions and merons in chiral liquid crystals and magnets, Phys. Rev. E **97**, 062706 (2018).

[23] S. Afghah and J. V. Selinger, Theory of helicoids and skyrmions in confined cholesteric liquid crystals, Phys. Rev. E **96**, 012708 (2017).

[24] M. N. Wilson, A. B. Butenko, A. N. Bogdanov, and T. L. Monchesky, Chiral skyrmions in cubic helimagnet films: The role of uniaxial anisotropy, Phys. Rev. B **89**, 094411 (2014).

[25] A. O. Leonov, T. L. Monchesky, N. Romming, A. Kubetzka, A. N. Bogdanov, and R. Wiesendanger, The properties of isolated chiral skyrmions in thin magnetic films, New J. Phys. **18**, 065003 (2016).

[26] M. T. Johnson, P. J. H. Bloemen, F. J. A. den Broeder, and J. J. de Vries, Magnetic anisotropy in metallic multilayers, Rep. Prog. Phys. **59**, 1409 (1996).

[27] S. D. Bader, Magnetism in low dimensionality, Surf. Sci. **500**, 172 (2002).

[28] L. Neel, Anisotropie magnetique superficielle et surstructures d'orientation, J. Phys. Radium **15**, 225 (1954).

[29] H. R. O. Sohn, C. D. Liu, and I. I. Smalyukh, Schools of skyrmions with electrically tunable elastic interactions, Nat. Commun. **10**, 4744 (2019).

[30] A. O. Leonov, I. E. Dragunov, U. K. Rößler, and A. N. Bogdanov, Theory of skyrmion states in liquid crystals, Phys. Rev. E **90**, 042502 (2014).

[31] A. Nych, J. Fukuda, U. Ognysta, S. Zumer, and I. Musevic, Spontaneous formation and dynamics of half-skyrmions in a chiral liquid-crystal film, Nat. Phys. **13**, 1215 (2017).

[32] H. R. O. Sohn, C. D. Liu, Y. Wang, and I. I. Smalyukh, Light-controlled skyrmions and torons as reconfigurable particles, Opt. Express **27**, 29056 (2019).

[33] P. J. Ackerman, T. Boyle, and I. I. Smalyukh, Squirming motion of baby skyrmions in nematic fluids, Nat. Commun. **8**, 673 (2017).

[34] A. Mertelj, D. Lisjak, M. Drofenik, and M. Copic, Ferromagnetism in suspensions of magnetic platelets in liquid crystal, Nature (London) **504**, 237 (2013).

[35] Q. Liu, P. J. Ackerman, T. C. Lubensky, and I. I. Smalyukh, Biaxial ferromagnetic liquid crystal colloids, Proc. Natl. Acad. Sci. USA **113**, 10479 (2016).

[36] P. Bak and M. H. Jensen, Theory of helical magnetic structures and phase transitions in MnSi and FeGe, J. Phys. C: Solid State Phys. **13**, L881 (1980).

[37] A. O. Leonov and A. N. Bogdanov, Crossover of skyrmion and helical modulations in noncentrosymmetric ferromagnets, New J. Phys. **20**, 043017 (2018).

[38] B. Schaub and D. Mukamel, Phase diagrams of systems exhibiting incommensurate structures, Phys. Rev. B **32**, 6385 (1985).

[39] J.-S. B. Tai and I. I. Smalyukh, Surface anchoring as a control parameter for stabilizing torons, skyrmions, twisted walls, fingers, and their hybrids in chiral nematics, Phys. Rev. E **101**, 042702 (2020).

[40] J. Rowland, S. Banerjee, and M. Randeria, Skyrmions in chiral magnets with Rashba and Dresselhaus spin-orbit coupling, Phys. Rev. B **93**, 020404(R) (2016).

[41] A. O. Leonov, C. Pappas, and I. I. Smalyukh, Field-driven metamorphoses of isolated skyrmions within the conical state of cubic helimagnets, Phys. Rev. B **104**, 064432 (2021).

[42] C. Andreas, A. Kakay, and R. Hertel, Magnon modes for a magnetic disc in a cone vortex state, Phys. Rev. B **89**, 134403 (2014).

[43] Y. Li, L. Pierobon, M. Charilaou, H.-B. Braun, N. R. Walet, J. F. Löffler, J. J. Miles, and C. Moutafis, Tunable terahertz oscillation arising from Bloch-point dynamics in chiral magnets, Phys. Rev. Research **2**, 033006 (2020).

[44] M. Charilaou, Prediction of confined and controllable Bloch points in nanocubes of chiral magnets, Phys. Rev. B **102**, 014430 (2020).

[45] C. A. Condat, R. A. Guyer, and M. D. Miller, Double sine-Gordon chain, Phys. Rev. B **27**, 474 (1983).

[46] D. K. Campbell, M. Peyrard, and P. Sodano, Kink-antikink interactions in the double sine-Gordon equation, Physica D **19**, 165 (1986).

[47] S. A. Meynell, M. N. Wilson, H. Fritzsche, A. N. Bogdanov, and T. L. Monchesky, Surface twist instabilities and skyrmion states in chiral ferromagnets, Phys. Rev. B **90**, 014406 (2014).

[48] D. McGrouther, R. J. Lamb, M. Krajnak, S. McFadzean, S. McVitie, R. L. Stamps *et al.*, Internal structure of hexagonal skyrmion lattices in cubic helimagnets, New J. Phys. **18**, 095004 (2016).

[49] D. Wolf, S. Schneider, U. K. Rößler, A. Kovacs, M. Schmidt, R. E. Dunin-Borkowski, B. Büchner, B. Rellinghaus, and A. Lubk, Unveiling the three-dimensional spin texture of skyrmion tubes, arXiv:2101.12630.

[50] S. Schneider, D. Wolf, M. J. Stolt, S. Jin, D. Pohl, B. Rellinghaus, M. Schmidt, B. Büchner, S. T. B. Goennenwein, K. Nielsch, and A. Lubk, Induction Mapping of the 3D-Modulated Spin Texture of Skyrmions in Thin Helimagnets, Phys. Rev. Lett. **120**, 217201 (2018).

[51] M. T. Birch, D. Cortés-Ortuño, L. A. Turnbull, M. N. Wilson, F. Groß, N. Träger, A. Laurenson, N. Bukin, S. H. Moody, M. Weigand, G. Schütz, H. Popescu, R. Fan, P. Steadman, J. A. T. Verezhak, G. Balakrishnan, J. C. Loudon, A. C. Twitchett-Harrison, O. Hovorka, H. Fangohr, F. Y. Ogrin *et al.*, Real-space imaging of confined magnetic skyrmion tubes, Nat. Commun. **11**, 1726 (2020).

[52] A. O. Leonov, T. L. Monchesky, J. C. Loudon, and A. N. Bogdanov, Three-dimensional chiral skyrmions with attractive interparticle interactions, J. Phys.: Condens. Matter **28**, 35LT01 (2016).

[53] J. C. Loudon, A. O. Leonov, A. N. Bogdanov, M. C. Hatnean, and G. Balakrishnan, Direct observation of attractive skyrmions and skyrmion clusters in the cubic helimagnet Cu_2OSeO_3, Phys. Rev. B **97**, 134403 (2018).

[54] H. Du, X. Zhao, F. N. Rybakov, A. B. Borisov, S. Wang, J. Tang, C. Jin, C. Wang, W. Wei, N. S. Kiselev, Y. Zhang, R. Che, S. Blügel, and M. Tian, Interaction of Individual Skyrmions in a Nanostructured Cubic Chiral Magnet, Phys. Rev. Lett. **120**, 197203 (2018).

[55] D. Capic, D. A. Garanin, and E. M. Chudnovsky, Skyrmion-skyrmion interaction in a magnetic film, J. Phys.: Condens. Matter **32**, 415803 (2020).

[56] A. O. Leonov, Y. Togawa, T. L. Monchesky, A. N. Bogdanov, J. Kishine, Y. Kousaka, M. Miyagawa, T. Koyama, J. Akimitsu, Ts. Koyama, K. Harada, S. Mori, D. McGrouther, R. Lamb, M. Krajnak, S. McVitie, R. L. Stamps, and K. Inoue, Chiral Surface Twists and Skyrmion Stability in Nanolayers of Cubic Helimagnets, Phys. Rev. Lett. **117**, 087202 (2016).

[57] A. O. Leonov and I. Kezsmarki, Asymmetric isolated skyrmions in polar magnets with easy-plane anisotropy, Phys. Rev. B **96**, 014423 (2017).

[58] D. Capic, D. A. Garanin, and E. M. Chudnovsky, Skyrmions in an oblique field, J. Magn. Magn. Mater. **537**, 168215 (2021).

[59] C. Wang, H. Du, X. Zhao, C. Jin, M. Tian, Y. Zhang, and R. Che, Enhanced stability of the magnetic skyrmion lattice phase under a tilted magnetic field in a two-dimensional chiral magnet, Nano Lett. **17**, 2921 (2017).

[60] A. O. Leonov and K. Inoue, Homogeneous and heterogeneous nucleation of skyrmions in thin layers of cubic helimagnets, Phys. Rev. B **98**, 054404 (2018).

[61] G. P. Müller, F. N. Rybakov, H. Jonsson, S. Blügel, and N. S. Kiselev, Coupled quasimonopoles in chiral magnets, Phys. Rev. B **101**, 184405 (2020).

[62] F. N. Rybakov, A. B. Borisov, and A. N. Bogdanov, Three-dimensional skyrmion states in thin films of cubic helimagnets, Phys. Rev. B **87**, 094424 (2013).

[63] F. N. Rybakov, A. B. Borisov, S. Bluegel, and N. S. Kiselev, New spiral state and skyrmion lattice in 3D model of chiral magnets, New J. Phys. **18**, 045002 (2016).

[64] Y. Togawa, T. Koyama, K. Takayanagi, S. Mori, Y. Kousaka, J. Akimitsu, S. Nishihara, K. Inoue, A. S. Ovchinnikov, and J. Kishine, Chiral Magnetic Soliton Lattice on a Chiral Helimagnet, Phys. Rev. Lett. **108**, 107202 (2012).

[65] A. O. Leonov, I. M. Tambovtcev, I. S. Lobanov, and V. M. Uzdin, Stability of in-plane and out-of-plane chiral skyrmions in epitaxial MnSi (111)/Si (111) thin films: Surface twists versus easy-plane anisotropy, Phys. Rev. B **102**, 174415 (2020).

[66] I. I. Smalyukh, B. I. Senyuk, P. Palffy-Muhoray, O. D. Lavrentovich, H. Huang, E. C. Gartland, V. H. Bodnar, T. Kosa, and B. Taheri, Electric-field-induced nematic-cholesteric transition and three-dimensional director structures in homeotropic cells, Phys. Rev. E **72**, 061707 (2005).

[67] N. Sisodia, P. K. Muduli, N. Papanicolaou, and S. Komineas, Chiral droplets and current-driven motion in ferromagnets, Phys. Rev. B **103**, 024431 (2021).

[68] F. N. Rybakov, A. B. Borisov, S. Blügel, and N. S. Kiselev, New Type of Stable Particlelike States in Chiral Magnets, Phys. Rev. Lett. **115**, 117201 (2015).

[69] Y. Zhou, E. Iacocca, A. A. Awad, R. K. Dumas, F. C. Zhang, H. B. Braun, and J. Akerman, Dynamically stabilized magnetic skyrmions, Nat. Commun. **6**, 8193 (2015).

[70] A. Hubert and R. Schaefer, *Magnetic Domains* (Springer, Berlin, 1998).

[71] Y. Ishikawa and M. Arai, Magnetic phase diagram of MnSi near critical temperature studied by neutron small angle scattering, J. Phys. Soc. Jpn. **53**, 2726 (1984).

[72] K. Kadowaki, K. Okuda, and M. Date, Magnetization and magnetoresistance of MnSi, J. Phys. Soc. Jpn. **51**, 2433 (1982).

[73] C. Pappas, E. Lelievre-Berna, P. Falus, P. M. Bentley, E. Moskvin, S. Grigoriev, P. Fouquet, and B. Farago, Chiral Paramagnetic Skyrmion-like Phase in MnSi, Phys. Rev. Lett. **102**, 197202 (2009).

[74] S. Buhrandt and L. Fritz, Skyrmion lattice phase in three-dimensional chiral magnets from Monte Carlo simulations, Phys. Rev. B **88**, 195137 (2013).

[75] I. Levatic, P. Popcevic, V. Surija, A. Kruchkov, H. Berger, A. Magrez, J. S. White, H. M. Ronnow, and I. Zivkovic, Dramatic pressure-driven enhancement of bulk skyrmion stability, Sci. Rep. **6**, 21347 (2016).

[76] Y. Okamura, F. Kagawa, S. Seki, and Y. Tokura, Transition to and from the skyrmion lattice phase by electric fields in a magnetoelectric compound, Nat. Commun. **7**, 12669 (2016).

[77] J. S. White, K. Prsa, P. Huang, A. A. Omrani, I. Zivkovic, M. Bartkowiak, H. Berger, A. Magrez, J. L. Gavilano, G. Nagy, J. Zang, and H. M. Ronnow, Electric-Field-Induced Skyrmion Distortion and Giant Lattice Rotation in the Magnetoelectric Insulator Cu_2OSeO_3, Phys. Rev. Lett. **113**, 107203 (2014).

[78] A. J. Kruchkov, J. S. White, M. Bartkowiak, I. Zivkovic, A. Magrez, and H. M. Ronnow, Direct electric field control of the skyrmion phase in a magnetoelectric insulator, Sci. Rep. **8**, 10466 (2018).

[79] J. S. White, I. Zivkovic, A. J. Kruchkov, M. Bartkowiak, A. Magrez, and H. M. Ronnow, Electric-Field-Driven Topological Phase Switching and Skyrmion-Lattice Metastability in Magnetoelectric Cu_2OSeO_3, Phys. Rev. Applied **10**, 014021 (2018).

[80] F. Qian, L. J. Bannenberg, H. Wilhelm, G. Chaboussant, L. M. DeBeer-Schmitt, M. P. Schmidt, A. Aqeel, T. T. M. Palstra, E. H. Bruck, A. J. E. Lefering, C. Pappas, and M. Mostovoy, New magnetic phase of the chiral skyrmion material Cu_2OSeO_3, Sci. Adv. **4**, eaat7323 (2018).

[81] A. Chacon, L. Heinen, M. Halder, A. Bauer, W. Simeth, S. Muehlbauer, H. Berger, M. Garst, A. Rosch, and C. Peiderer, Observation of two independent skyrmion phases in a chiral magnetic material, Nat. Phys. **14**, 936 (2018).

[82] X. Z. Yu, Y. Onose, N. Kanazawa, J. H. Park, J. H. Han, Y. Matsui, N. Nagaosa, and Y. Tokura, Real-space observation of a two-dimensional skyrmion crystal, Nature (London) **465**, 901 (2010).

[83] X. Z. Yu, N. Kanazawa, Y. Onose, K. Kimoto, W. Z. Zhang, S. Ishiwata, Y. Matsui, and Y. Tokura, Near room-temperature formation of a skyrmion crystal in thin-films of the helimagnet FeGe, Nat. Mater. **10**, 106 (2011).

[84] J. Tang, Y. Wu, W. Wang, L. Kong, B. Lv, W. Wei, J. Zang, M. Tian, and H. Du, Magnetic skyrmion bundles and their current-driven dynamics, Nat. Nanotechnol. (2021), doi:10.1038/s41565021009549.

[85] N. Romming, C. Hanneken, M. Menzel, J. E. Bickel, B. Wolter, K. von Bergmann, A. Kubetzka, and R. Wiesendanger, Writing and deleting single magnetic skyrmions, Science **341**, 636 (2013).

[86] N. Romming, A. Kubetzka, C. Hanneken, K. von Bergmann, and R. Wiesendanger, Field-Dependent Size and Shape of Single Magnetic Skyrmions, Phys. Rev. Lett. **114**, 177203 (2015).

[87] J. Müller, Magnetic skyrmions on a two-lane racetrack, New J. Phys. **19**, 025002 (2017).

[88] W. Kang, Y. Huang, C. Zheng, W. Lv, Na Lei, Y. Zhang, X. Zhang, Y. Zhou, and W. Zhao, Voltage controlled magnetic skyrmion motion for racetrack memory, Sci. Rep. **6**, 23164 (2016).

[89] X. Zhang, G. P. Zhao, H. Fahngohr, J. Ping Liu, W. X. Xia, J. Xia, and F. J. Morvan, Skyrmion-skyrmion and skyrmion-edge repulsions in skyrmion-based racetrack memory, Sci. Rep. **5**, 7643 (2015).

[90] M. Kawachi, O. Kogure, and Y. Kato, Bubble domain texture of a liquid crystal, Jpn. J. Appl. Phys. **13**, 1457 (1974).

[91] W. E. L. Haas and J. E. Adams, Electrically variable diffraction in spherulitic liquid crystals, Appl. Phys. Lett. **25**, 263 (1974).

[92] I. I. Smalyukh, Y. Lansac, N. A. Clark, and R. P. Trivedi, Three-dimensional structure and multistable optical switching of triple-twisted particle-like excitations in anisotropic fluids, Nat. Mater. **9**, 139 (2010).

[93] M. B. Pandey, T. Porenta, J. Brewer, A. Burkart, S. Copar, S. Zumer, and I. I. Smalyukh, Self-assembly of skyrmion-dressed chiral nematic colloids with tangential anchoring, Phys. Rev. E **89**, 060502(R) (2014).

[94] Y. A. Kharkov, O. P. Sushkov, and M. Mostovoy, Bound States of Skyrmions and Merons near the Lifshitz Point, Phys. Rev. Lett. **119**, 207201 (2017).

[95] H. R. O. Sohn, S. M. Vlasov, V. M. Uzdin, A. O. Leonov, and I. I. Smalyukh, Real-space observation of skyrmion clusters with mutually orthogonal skyrmion tubes, Phys. Rev. B **100**, 104401 (2019).